A new clinical unit for digital radiography based on a thick amorphous Selenium plate: Physical and psychophysical characterization

Stefano Rivetti
Alma Mater Studiorum, Physics Department, University of Bologna, 40127 Bologna, Italy and S.C. di Fisica Sanitaria "Azienda USL di Modena" 41100 Modena, Italy

Nico Lanconelli[a)]
Alma Mater Studiorum, Physics Department, University of Bologna, 40127 Bologna, Italy

Marco Bertolini
Arcispedale Santa Maria Nuova, 42123 Reggio Emilia, Italy

Domenico Acchiappati
S.C. di Fisica Sanitaria "Azienda USL di Modena" 41100 Modena, Italy

(Received 12 October 2010; revised 8 June 2011; accepted for publication 9 June 2011; published 21 July 2011)

Purpose: Here, we present a physical and psychophysical characterization of a new clinical unit (named AcSelerate) for digital radiography based on a thick a-Se layer. We also compared images acquired with and without a software filter (named CRF) developed for reducing sharpness and noise of the images and making them similar to images coming from traditional computed radiography systems.
Methods: The characterization was achieved in terms of physical figures of merit [modulation transfer function (MTF), noise power spectra (NPS), detective quantum efficiency (DQE)], and psychophysical parameters (contrast-detail analysis with an automatic reading of CDRAD images). We accomplished measurements with four standard beam conditions: RAQ3, RQA5, RQA7, and RQA9.
Results: The system shows an excellent MTF (about 50% at the Nyquist frequency). The DQE is about 55% at 0.5 lp/mm and above 20% at the Nyquist frequency and is almost independent from exposure. The contrast-detail curves are comparable to some of the best published data for other systems devoted to imaging in general radiography. The CRF filter influences both the MTF and NPS, but it does lead to very small changes on DQE. Also the visibility of CDRAD details is basically unaltered, when the filter is activated.
Conclusions: As normally happens with detector based on direct conversion, the system presents an excellent MTF. The improved efficiency caused by the thick layer allows getting good noise characteristics and DQE results better (about 10% on average) than many of the computed radiography (CR) systems and comparable to those obtained by the best systems for digital radiography available on the market. [DOI: 10.1118/1.3605471]

Key words: digital radiology, direct conversion detector, amorphous selenium.

I. INTRODUCTION

Digital radiography techniques are playing an important role in the recent progress of x-ray imaging systems devoted to general radiography. In the last decade, flat panel detectors based on a-Si active matrix thin-film transistor (TFT) readout technology became commercially available.[1,2] The TFT array is coupled with an x-ray absorption layer which is integral in converting the x-rays to a usable signal. Depending on the type of detector, the conversion of x-rays into electric signals is either direct or indirect. Direct x-ray flat-panel systems normally use a layer of amorphous Selenium (a-Se), whereas indirect conversion flat-panel detectors are typically based on a cesium iodide phosphor layer. Systems based on a-Se have excellent spatial resolution and are well suited for mammography, where the use of low energy x-rays permits good quantum efficiency (QE) with relatively thin a-Se layers. However, in general radiography, including chest radiography, much higher x-ray energies are used and the QE of the relatively low atomic number a-Se layers is poorer, making a-Se systems less well suited for chest radiography.[3,4]

To overcome this problem a new a-Se direct conversion detector for digital radiography has recently been introduced into the digital radiography market.[5] This system, manufactured by FUJIFILM and named AcSelerate, makes use of a fullerene (C60)-doped polymer layer placed on a thick a-Se layer (1000 μm) coupled to an a-Si TFT array. The C-60 doped polymer layer should lead to improved lag characteristics and is supposed to prevent the crystallization of a-Se.[5] Further, the thick a-Se layer should help to improve the overall efficiency of the system by decreasing its noise and keeping a very good spatial resolution at the same time. The QE of this detector, as derived from Monte Carlo simulations, is 93, 75, 58, and 41%, for the RQA3, RQA5, RQA7, and RQA9 beams, respectively.

For getting a characterization of a digital detector from a physical point of view, we can estimate several features. Image quality is often assessed by the measurements of figures such as modulation transfer function (MTF), noise power spectra (NPS), and detective quantum efficiency (DQE). These metrics have been found to be very helpful for measuring in an objective way features as spatial resolution, contrast, and noise. The quality of a clinical system may be characterized using these objective measures, however, medical diagnosis often involves the perception of medium and small details lying on an anatomical background. From this perspective, one can also characterize an imaging system by investigating its performance in the perception of known details on a given background. In recent years, various phantoms have been developed for the assessment of the contrast-detail (CD) visibility of predetermined details with various sizes and contrasts. Among these, the CDRAD phantom is often employed for getting a 4-alternative forced choice (4-AFC) response for systems used in general radiography. Although results obtained with CD studies could not be directly extended to clinical detection tasks, CD analysis is still a step forward in the examination of details resembling clinical lesions. Having said this, the combination of physical measurements and CD analysis allows the achievement of a more complete evaluation of an imaging system.

The aim of this paper is to achieve a characterization of a new clinical unit for digital radiography based on a direct conversion detector (named FUJIFILM FDR AcSelerate), through physical figures of merit (MTF, NPS, and DQE), and psychophysical parameters (CD analysis). We also compared images acquired with and without a new software filter (named CRF) developed by FUJIFILM for reducing sharpness and noise of the images and make them similar to images coming from traditional computed radiography (CR) systems.

II. MATERIALS AND METHODS

Table I summarizes the main characteristics of the investigated system. A wide range of uniform exposures were used to calculate the system response curve. The average pixel value was estimated from a region of interest (ROI) located at the center of the detector. We then performed a characterization of the FUJIFILM AcSelerate unit, by measuring both physical properties, such as MTF, NPS, DQE, and psychophysical figures (CD analysis). The images were acquired after removing the system cover, the antiscatter grid, and the automatic exposure control (AEC) chambers. The DQE was estimated according to the international standard IEC 62220-1.[6] We acquired images by considering four different standard beam conditions: RQA3, 5, 7, and 9, according to IEC-61267 standard.[7] We measured the exposure to the detector with a calibrated ionization chamber (UNFORS Xi, Unfors Instruments, Billdal, Sweden). The source-to-image distance was about 180 cm. AcSelerate employs the usual image processing technology used by FUJIFILM for their CR systems. In fact, users are required to choose among one of the processing methods (automatic, semi-automatic, FIX mode, and others). The FIX-mode is the only one that allows users to select the sensitivity (S) and latitude (L) values, such that the pixel values in the resultant image are directly linked to exposure in a manner that mimics a film screen system. All the images used in this work were acquired with the FIX-mode processing using the following two sets of reading process parameters: $S = 200$ and $L = 2$.

Given the very good spatial resolution of a-Se detectors, AcSelerate images are expected to present a very high sharpness. FUJIFILM has developed a software filter, which aims to modify the sharpness of the images coming from AcSelerate. This has been done in order to make them similar to images coming from traditional CR systems. In fact, the image processing tools available within the AcSelerate are the same present in all the CR manufactured by FUJIFILM, except for a new filter named CRF. This filter is supposed to provide better noise properties and the same unsharpness as CR. For users that prefer traditional CR images and dislike noisy images, the CRF filter should be activated. The default setting is "OFF", thus the CRF filter must be turned on by users through the acquisition console. The filter is integrated in the acquisition software (CRF option), and the user can decide to view images with or without it. The CRF filter is available only on the acquisition console. Once the image is acquired, one can decide to apply or not apply the filter, even after the acquisition, provided that this procedure must be done on the acquisition console. Thus, images with or without the CRF filter come out from the same acquisition, and the data can be postprocessed at any time on the acquisition console. This filter, as will be shown, influences both the signal and noise power spectra in almost the same proportion, leading to only small changes in the DQE.

TABLE I. Main characteristics of the investigated system.

Manufacturer	FUJIFILM
System	AcSelerate
Detection type	Direct conversion
Detector material	aSe
Detector thickness [μm]	1000
Imaging area [cm $\times$ cm]	43×43
Array size	2880×2880
Pixel pitch [μm]	150
Image depth [bits]	12

II.A. Physical characterization

Firstly we determined the response curve of the system for all the investigated beams by acquiring images within a wide range of uniform x-ray exposures. The response curves were fitted with a logarithmic function and used for linearizing all the acquired images. We measured the presampling MTF with the edge technique: an oversampled edge spread function was obtained by a tungsten edge test device (TX5, IBA Dosimetry, Schwarzenbruck, Germany). We estimated the MTFs both in the horizontal and vertical directions. We then averaged the MTF along the two directions for

calculating the final DQE. NPS was computed by acquiring flood images at various exposure levels ranging from 1 to more than 10 μGy. For each exposure, the 2D NPS was obtained from averaging the Fourier transformations of fixed-size ROIs extracted from four different images. The 1D NPS was then extracted from the 2D NPS on a radial direction at 45°, excluding the values along the axes. For a more complete evaluation of the noise properties of the detector, we also implemented the relative standard deviation (RSD) analysis.[8] We estimated the RSD on the same ROIs used for NPS calculation. The RSD squared data measured at each exposure were fitted with the following function:

$$RSD^2 = \left(\frac{\sigma_{TOT}}{x}\right)^2 = \frac{\alpha}{x} + \beta + \frac{\gamma}{x^2}. \quad (1)$$

Here, x represents the x-ray exposure, while the three coefficients α, β, and γ indicates the contributions of the quantum-statistical (Poisson) noise source, of a dose related (multiplicative) noise source, and of a dose independent (additive) noise source, respectively. Usually, the additive component is connected to electronic noise (e.g., dark current). On the other hand, the multiplicative component might be due to a structured noise arising from variations in sensitivity across the detector. The RSD is obtained on images linearized by means of the response curves. As a consequence, the RSD itself is dimensionless, and the units for the three coefficients are those shown in Table II. For each considered x-ray beam, we used tabulated data for the photon fluence.[6] The final DQE is then calculated as:

$$DQE(f) = \frac{MTF^2(f)}{NPS(f,q)\cdot q} \quad (2)$$

where q is the number of photons per unit area.

II.B. Contrast-detail analysis

The psychophysical characterization was assessed by performing a contrast-detail analysis with an automatic reading of CDRAD 2.0 (Artinis, Medical Systems B.V., Zetten, The Netherlands) images. For each exposure level four images were acquired. The exposure values were the same as those used for the physical characterization, this with the implicit assumption that the x-ray absorption for the CDRAD phantom was about 25%. The phantom was repositioned after each exposure.

TABLE II. Values of the main noise components for the four x-ray beams, as estimated by RSD analysis. For each component, the top row represents values for images acquired without the filter, whereas the bottom row represents values for images acquired with the filter enabled.

Components	RQA3	RQA5	RQA7	RQA9
Poisson: α (μGy)	2.2×10^{-3}	2.1×10^{-3}	2.3×10^{-3}	3.2×10^{-3}
	4.9×10^{-4}	5.2×10^{-4}	4.1×10^{-4}	5.5×10^{-4}
Multiplicative: β	1.0×10^{-6}	1.0×10^{-5}	1.0×10^{-7}	3.6×10^{-6}
	7.7×10^{-7}	2.0×10^{-7}	1.0×10^{-7}	6.3×10^{-6}
Additive: γ (μGy^2)	1.2×10^{-3}	6.7×10^{-4}	9.1×10^{-4}	1.1×10^{-3}
	6.6×10^{-5}	5.0×10^{-5}	2.2×10^{-4}	3.9×10^{-4}

The CD analysis was carried out in two different ways: with human observers and with software which performs an automatic reading. Human observers evaluated images on two dedicated high resolution reference monitors (Barco MGD521, 2048×2560 matrix, 8 bit, max luminance: 600 cd/m^2). The visualization parameters (brightness, contrast, and magnification factor) were fixed at the same value for all the observers. Readers have all the time they need for reading each phantom image. Five experienced operators evaluated the phantom images by using a dedicated software developed by our group and freely available at www.df.unibo.it/medphys. For each reading of the phantom a CD curve was computed, by fitting the reading data with a Weibull function.

The reading of CDRAD phantoms by human observers presents two main drawbacks. First, remarkable interobserver errors can arise. Second, the human reading is very time consuming. In order to surpass these weaknesses, automatic methods can be used for getting contrast-detail results from phantom images. Our group has also developed software that automatically reads the CDRAD images which is written in IDL™ (ITTVIS, Pearl East Circle Boulder, CO) and can be freely downloaded at www.df.unibo.it/medphys. Figure 1 shows the main panel of this software. The software scans all the cells of the phantom. For each cell shown in the left part of the graphical user interface (GUI) a few parameters for the central disk are estimated for obtaining the CD curve. Specifically, a few ROIs positioned within the details objects and on the background of the cell are used to calculate the signal-to-noise ratio (SNR) for each cell of the phantom. The noise is computed as the fluctuations of the background. We calculated SNR as the ratio between signal (contrast of the central

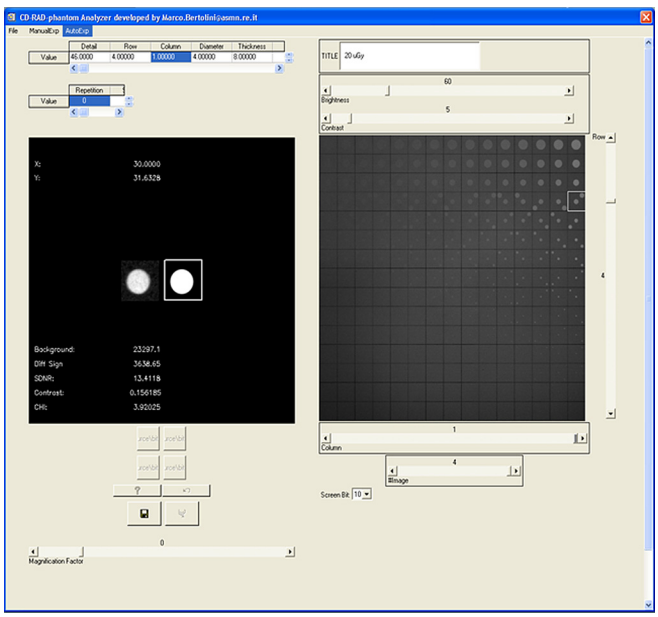

FIG. 1. The main panel of the GUI developed for the automatic reading of the CDRAD phantom images. The software scans all the cells of the CDRAD phantom, each time estimating some parameters for calculating the contrast-detail curve.

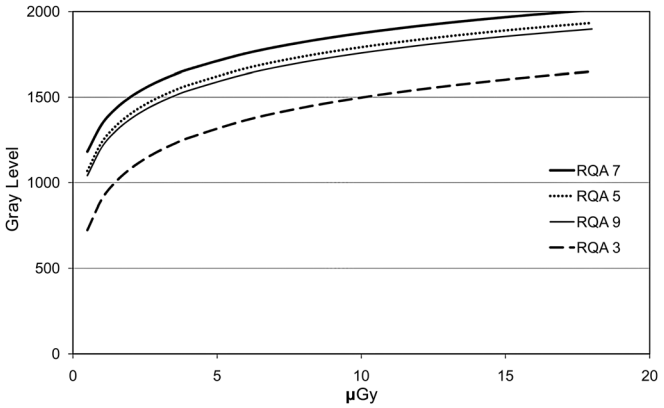

FIG. 2. Response curves for the four investigated beams (RQA3, RQA5, RQA7, and RQA9). The response is logarithmic for all the x-ray conditions and fittings were achieved with a $R^2 > 0.99$.

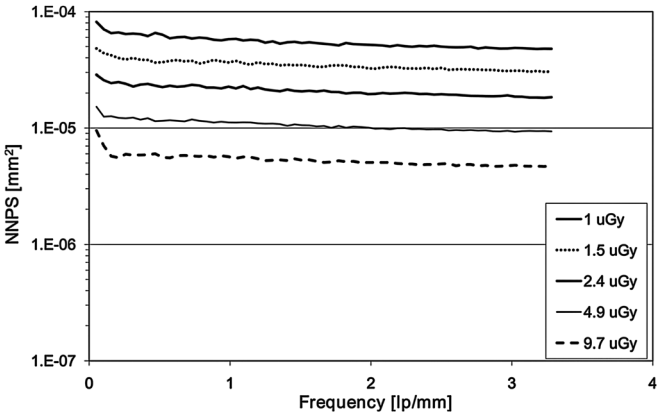

FIG. 4. NPS for the RQA5 beam at different exposures: 1D NPS was computed along a radial line of the 2D NPS. The system presents basically a white noise.

detail) and noise (standard deviation of the background near the detail). This corresponds to a direct measure of SNR. We apply the statistical detection theory (STD) without using MTF, NEQ and DQE information but the detection performance is directly calculated on the SNR (or observer's signal-to-noise ratio). This method takes into account spectral dependence that affects mean and standard deviation instead of considering MTF, NPS, and DQE. After having calculated the SNR for each cell of the CDRAD phantom, we computed a detectability index based on SNR and contrast, according to the ideal observer model in a SKE/BKE task. In practice, the detectability of the system is estimated as the ratio between the intrinsic contrast of the object and the estimated SNR. We estimated the contrast threshold of the CD curve as the abovementioned ratio, as derived by fitting the experimental data (SNR vs intrinsic contrast) for each diameter. For each exposure, a CD curve is obtained by averaging results of the four images acquired with that specific exposure. More details about the procedure used to estimating the automatic CD curves can be found in Refs. 9 and 10. In Ref. 9, SNR was described and estimated according to the matched filter theory. Here we exploited only the general equation: $C_T = SNR_T \cdot (C/SNR)$. We then fixed $SNR_T = 1$ and calculating the SNR directly from the images we then estimated the value of C_T. Unlike,[9] we computed the SNR as S/N with S as the disk contrast and N as the fluctuations in the background.

Since the AcSelerate system presents unfiltered images which have white noise, as can be seen in the "Results" section, in this case, the use of an automatic method for CD analysis based on pixel SNR is justified and will be used through this paper.[11] However, a final comparison gained with human observers is presented for images with and without the CRF filter. We also estimated the theoretical CD curves, as obtained by the well-known Rose model.[12] According to this model, for a circular target of diameter α, the contrast threshold (C_{TR}) can be calculated as:

$$C_{TR} = \frac{2k}{\alpha\sqrt{\pi \cdot q \cdot \mathrm{DQE}(0)}}. \quad (3)$$

Here DQE(0) is the DQE at zero spatial frequency and k represents the minimum SNR threshold needed by the observer for detecting the object.

We conducted a non parametric test (Mann-Whitney) to test if CD curves were significantly different by means of the SPSS package (version 13.0; SPSS Inc., Chicago, IL, USA). A p-value of less than 0.05 was considered to indicate a statistically significant difference between two curves.

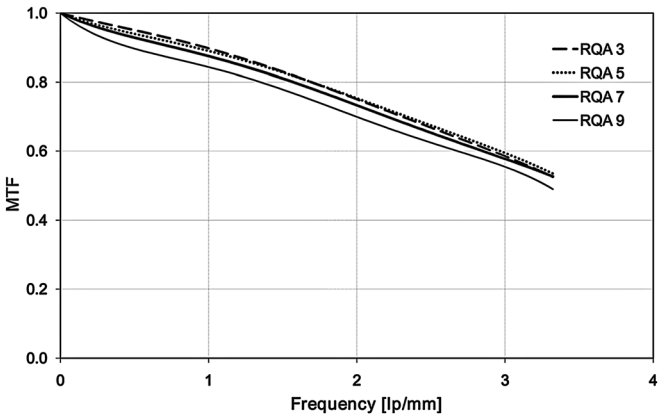

FIG. 3. MTF estimated with the edge technique for the four investigated beams. The four beams provide a similar MTF over the entire range of frequencies. We did not see appreciable differences between the MTF along the horizontal and vertical direction. Here we show the MTF resulting from the average on the two directions.

III. RESULTS

For each beam quality in the analyzed dose range, the response curves were fitted with a logarithmic function as shown in Fig. 2. All fittings were achieved with $R^2 > 0.99$. Note that, like most of the systems manufactured by FUJIFILM, the system presents a logarithmic behavior for all four beams.[13,14] All the subsequent measurements (both physical and psychophysical characterization) were then performed on linearized images.

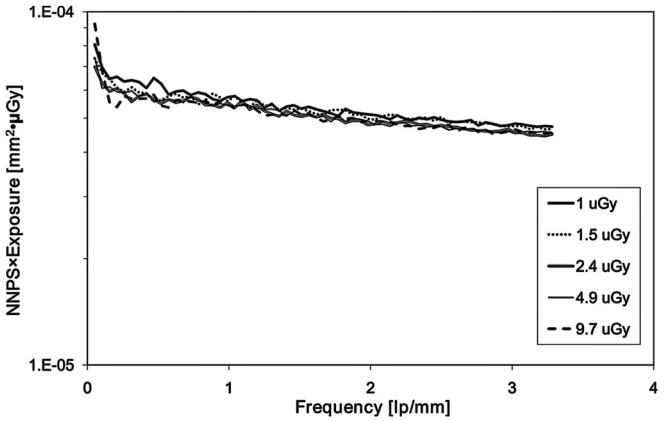

FIG. 5. NPS multiplied by air kerma for the RQA5 beam. This product should be independent from the exposure, for a strictly quantum noise limited detector.

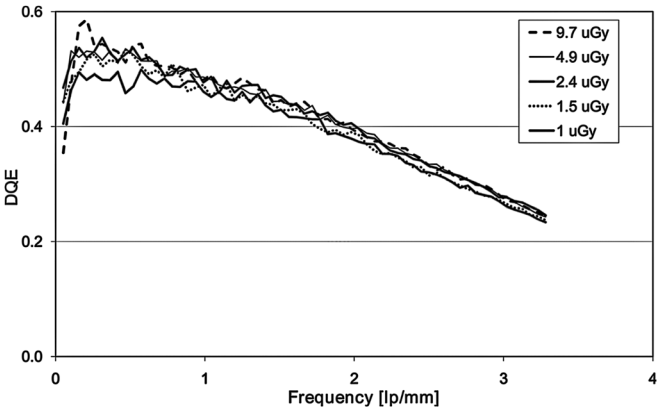

FIG. 7. DQE of the AcSelerate system for the RQA5 beam at various exposures. It is worth noting that the system presents a DQE almost independent from the exposure.

III.A. Physical characterization

In Fig. 3 are shown the MTF curves obtained for the four investigated beams, each made at an exposure of about 6 μGy. The plotted curves were obtained as the average of the MTFs estimated on the two orthogonal directions. The MTF was found to be almost independent of the beam quality and exposure level, at least in the range of investigated exposures (from 1 to 20 μGy). To calculate the DQE, the mean of the MTF along the two orthogonal directions was used.

Figure 4 shows the 1D NPS calculated for the RQA5 beam at various exposure levels. The NPS was estimated along a radial line at 45° from the principal axes.

For the RSD analysis, we used the same ROIs as were used in the NPS estimation. The experimental data were fitted with the function given in Eq. (1); the coefficients of the fitting functions are summarized in Table II for the four beams and images acquired with and without the CRF filter. These parameters correspond to the different noise components. The system presents a very small, nearly negligible, multiplicative component. Also, the additive component is smaller than the quantum component by about 1 order of magnitude under all investigated conditions. This behavior has been assessed over the entire range of investigated exposures (from about 1 to 10 μGy).

For a strictly quantum noise limited system, the product of the NPS and the exposure air kerma should remain constant for all exposures. Figures 5 and 6 illustrate this product for the RQA5 beam and for all the beams at an exposure of about 3 μGy, respectively. From Fig. 5, we may note that this product is basically constant for all the exposures, revealing that the detector is working in a quantum noise limited condition, at least within the range of investigated exposures. Figure 6 shows that the noise of the system changes with the beam energy. In particular, the most energetic beam (RQA9) presents a worse response.

In Fig. 7, we show the DQE for the RQA5 beam at various exposures. The AcSelerate presents a very high DQE (about 55% at 0.5 lp/mm and above 20% at the Nyquist frequency). Again, the DQE is essentially not affected by exposure, a typical feature of systems working in quantum noise limited conditions. In Fig. 8, we plot the DQE of the system for the four x-ray beams at an exposure of 3 μGy. As expected, the DQE of the system decreases as the average energy of the beam increases.

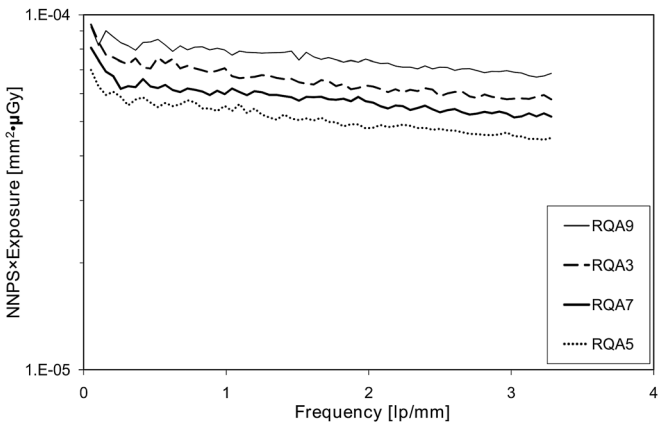

FIG. 6. NPS multiplied by air kerma for the four investigated beams at an exposure of about 3 μGy. We can note that the noise of the system changes with the beam energy.

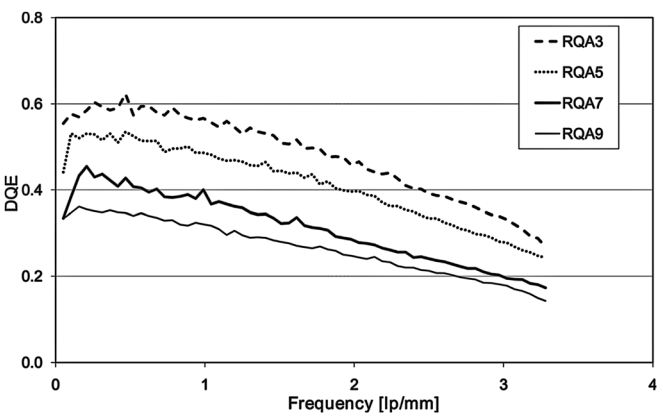

FIG. 8. DQE for the four beams at an exposure of about 3 μGy. As expected, the DQE of the system decreases as the energy of the x-ray beam increases.

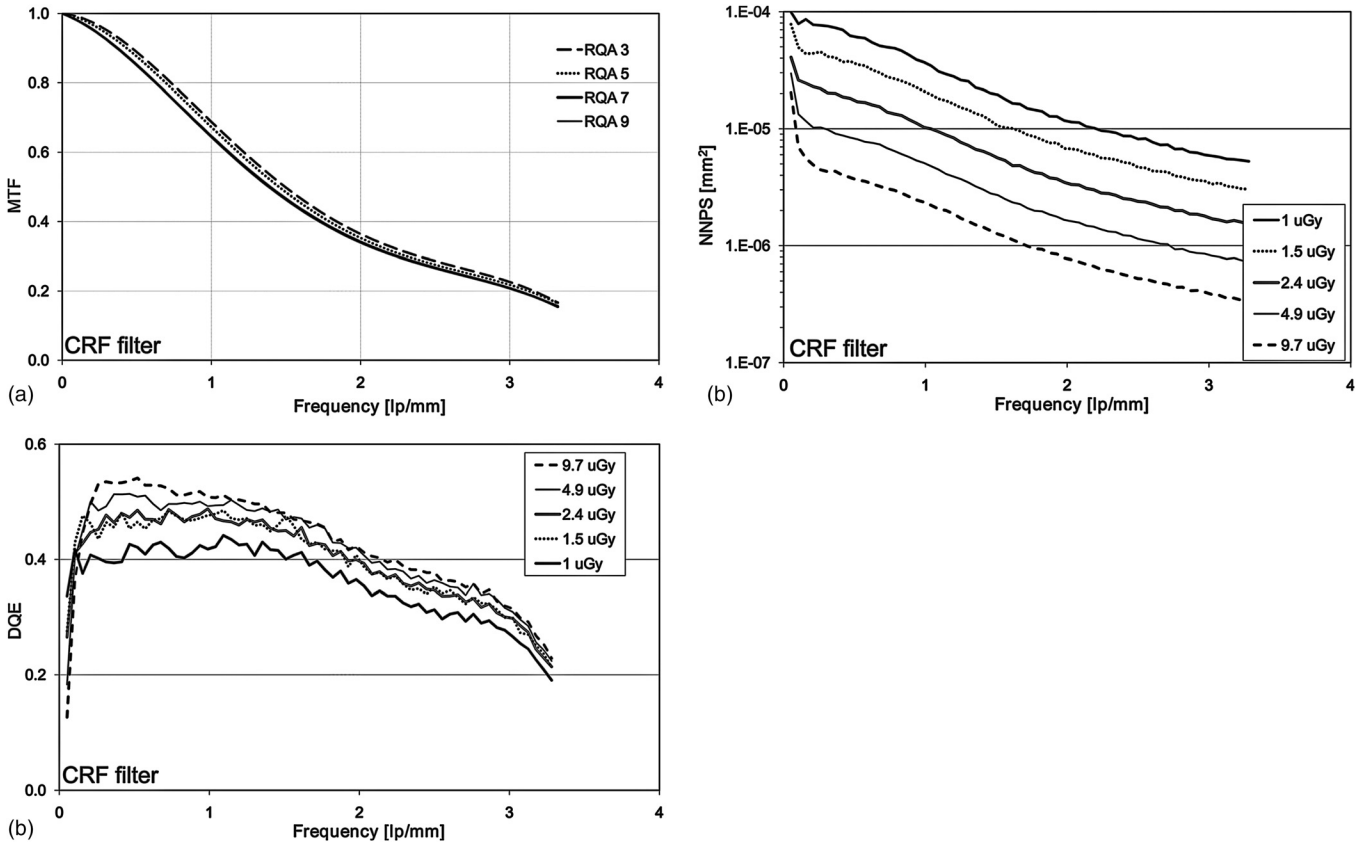

FIG. 9. MTF (a), NPS (b), and DQE (c) calculated on images acquired with the CRF filter. MTF was estimated for the four investigated beams. The CRF filter considerably affects the MTF, decreasing the spatial resolution of the system. NPS for the RQA5 beam at different exposures: in this case the system presents a noise decreasing with frequency. The DQE of the system has been calculated for the RQA5 beam at various exposures: here the outcomes seems to be slightly dependent from the exposure.

Figure 9 shows the MTF, NPS, and DQE of the AcSelerate system, calculated when the CRF filter was activated. In particular, Fig. 9(a) presents the MTF for the four investigated beams, whereas Figs. 9(b) and 9(c) illustrate the NPS and the DQE for the RQA5 beam at different exposures.

In Fig. 10, we present a picture of the 2D NPS for images with and without the CRF filter, calculated for RQA5 at 6 μGy. The system presents basically a white noise that becomes a noise decreasing with frequency when the CRF filter is enabled. Figure 11 shows an example of 1D NPS estimated for images acquired with the CRF filter on three different directions: horizontal, vertical, and along a radial line at 45° from the principal axes. While we cannot perceive any differences between the horizontal and vertical direction, the NPS estimated along the radial line is fairly different. For images acquired without the CRF filter, the noise estimated along the three directions is mostly the same. The same behavior can be observed for the other beams and exposure levels.

It is worth remarking that, even if the CRF filter affects in a considerable way both the MTF and the NPS, the DQE is basically unaltered by the activation of the filter. In fact, the difference between the DQE with and without filter is shown in Fig. 12 and, apart from the initial low-frequency drop region, it is on the order of some percents.

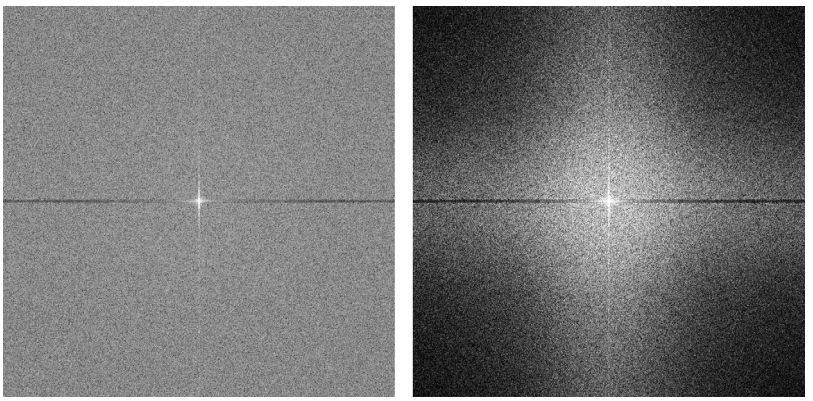

FIG. 10. Example of the 2D NPS for the RQA5 beam for images acquired at the same exposure with and without the CRF filter, respectively on the right and on the left. The effect of the filter is to reduce the high-frequency noise. It is worth noting that the contribution along the horizontal axis is lowered at almost all the frequencies. The same trend can be observed at different exposures and for the other investigated beams. The window-level of the images has been modified for having a better visualization.

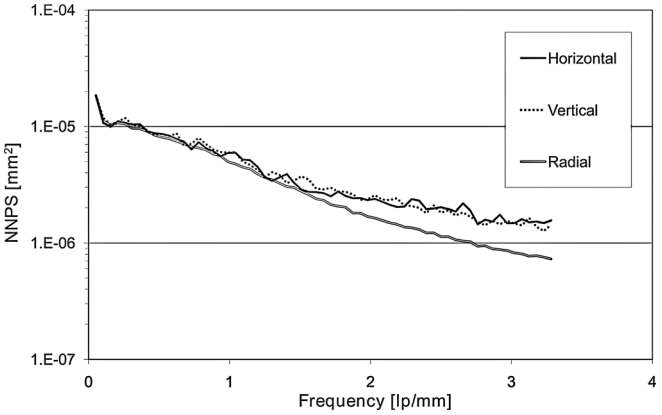

FIG. 11. 1D NPS for the RQA3 beam for the same exposure estimated on three different directions: horizontal, vertical, and along a radial line at 45° for images acquired with the CRF filter enabled.

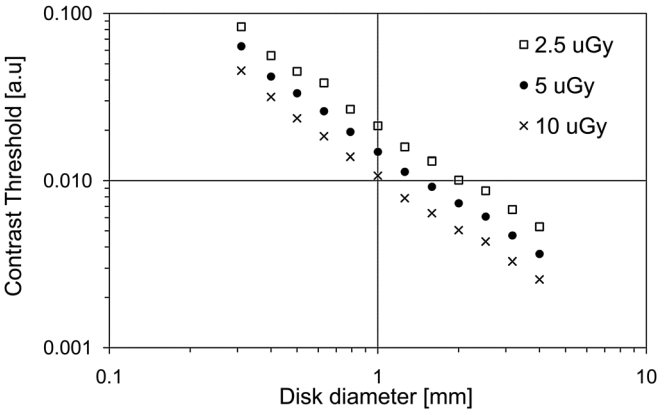

FIG. 13. Comparison of CD curves obtained with the automatic reading for the RQA5 beam at different exposures.

The presence of these small differences is due to the different values of MTF and NPS, as estimated with or without the CRF filter.

III.B. Contrast-detail analysis

In Fig. 13, we show the CD curves calculated with the automatic software for the RQA5 beam for three different exposures. As expected, the visibility of the details increases with exposure. Figure 14 illustrates the CD curves obtained for the four beams at an exposure of about 2.5 μGy. Although the difference is not statistically significant, the RQA9 beam provides a slightly worse response, with respect to the other beams.

In Fig. 15, we plotted three CD curves: one coming from experimental data for the AcSelerate system (RQA5 at 2.5 μGy), one theoretical curve calculated with the Rose model, and finally one of the best curve for other systems gathered from recent published data.[14] The CD response of the AcSelerate is in line with the best published data.

Figure 16 shows a comparison of the CD curves estimated by human observers for images acquired with the RQA5 beam at an exposure of about 2.5 μGy with and without the CRF filter. No statistically significant differences can be noticed.

IV. DISCUSSION

Although AcSelerate is a system based on direct conversion, its response curve is logarithmic, just as all the systems manufactured by FUJIFILM. Further, the response curve presents the lowest sensitivity for RQA3 beam and its maximum for RQA7 beam, as already noted and measured for other detectors.[15,16]

The system shows an excellent MTF, as direct conversion detectors usually do, in spite of the great thickness of its a-Se layer. In all the investigated conditions, we did not find appreciable differences between the MTF estimated in the horizontal and vertical direction.

The 2D NPS demonstrated to be a very useful tool, for a better understanding of the processing performed on the acquired images. We would like to note two remarkable points. Firstly, all the 2D spectra present very low values along the horizontal principal axis. These values appear along the entire axis, apart from a neighbor of the origin. Usually, for flat panels based on a-Se, at least one of the

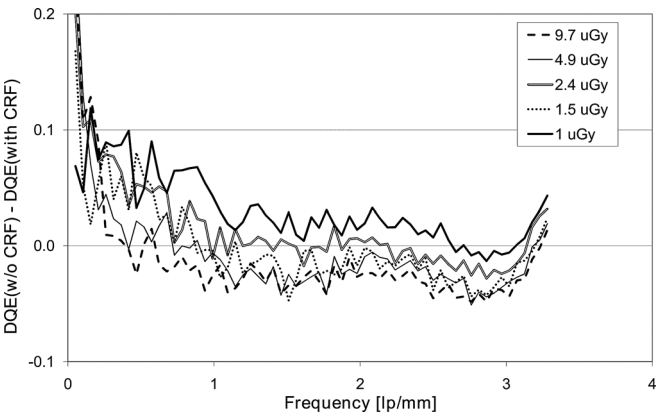

FIG. 12. Point-to-point difference between the DQE without and with the CRF filter for the RQA5 beam. It is worth noting that the CRF filter does not produce a noticeable impact on the DQE outcomes.

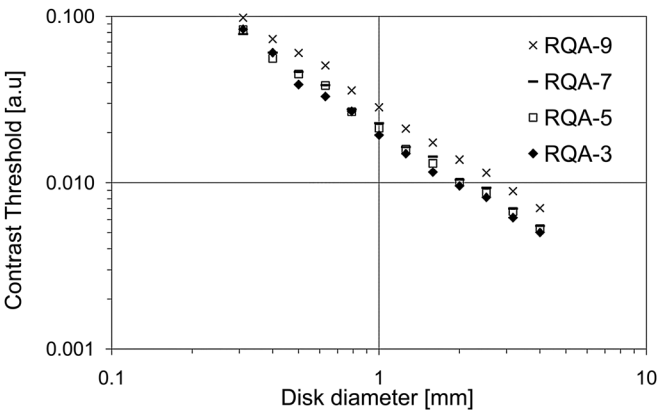

FIG. 14. Comparison of the CD curves obtained with the automatic reading for the four investigated beams at an exposure of about 2.5 μGy. The most energetic beam presents CD outcomes slightly worse than the other beams.

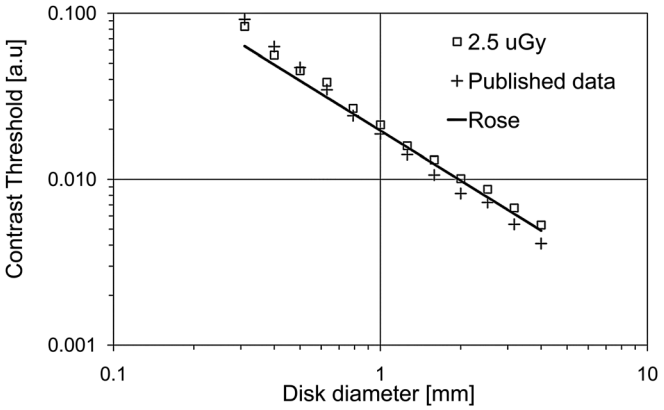

FIG. 15. Here we plotted the CD curves obtained at an exposure of about 2.5 μGy (RQA5 beam): images acquired without the CRF filter, theoretical Rose model [as described in Eq. (3)], and best results coming from published data for CR systems (Ref. 12).

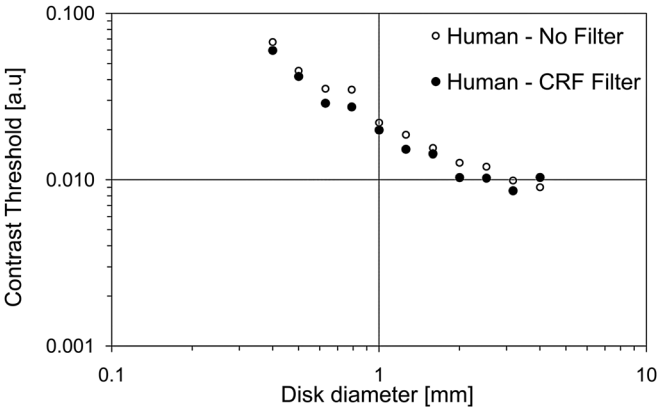

FIG. 16. Comparison of the CD curves estimated by human observers for images acquired with the RQA5 beam at an exposure of about 2.5 μGy with and without the CRF filter. No statistically significant differences can be noticed.

axes presents a higher noise. The noise contribution along the horizontal axis seems to be lowered through a filtering process by software for the AcSelerate system. A similar effect on 2D spectra was already observed in other systems developed by FUJIFILM.[13,14] Hence, even if we do not have many details from the manufacturer, we believe that this filter was designed to remove banding non uniformities in one of the principal directions. The second point is that, similarly to most of the systems based on direct conversion detectors, the AcSelerate shows a nearly uniform noise across the entire range of frequencies.[3,15,16] By comparing the RSD outcomes with those obtained on the latest CR systems,[14] it turned out that the AcSelerate presents noise components very similar to those of the other systems.

From the plots showing the product of the NPS and the exposure we can recognize that the investigated system is working in quantum noise limited condition within the range of investigated exposures. The tendency of the NPS curves is similar for all the investigated beam qualities. The noise of the system changes with energy, and the RQA9 beam, as expected, shows a slight worse performance probably due to the a-Se lower efficiency at high energies.[15,16]

Looking at the DQE curves, the first thing that is worth pointing out is that the AcSelerate unit, thanks to the great thickness of its a-Se layer, is able to provide very good DQE outcomes. In fact, they were found to be better than many other systems and comparable to those obtained by the best systems available on the market.[3,14–16] We can note that the DQE of the system decreases as the energy increases, probably caused by the lower efficiency of Selenium at high energies.

CD results are consistent to those obtained for the DQE calculation: for each exposure level the three beams RQA3, 5, and 7 provide comparable results, while RQA9 achieves, as expected, slightly worse results (highest CD curve). Finally, the performance of the AcSelerate unit, in terms of CD outcomes, is comparable to some of the best published data for other systems devoted to imaging in general radiography.

The activation of the CRF filter modifies some of the features of the images provided by the detector. First, the MTF diminishes considerably and becomes similar to many other systems available on the market.[14,15,17,18] The RSD analysis revealed that the CRF filter helps to reduce all the noise components, for all the considered x-ray beams. In this case, the AcSelerate system presents a noise in the proximity of the principal axes which is higher than the noise at frequencies far from the axes. Further, the noise is no longer isotropic; as a consequence, the 1D NPS is different if computed on two different directions. For instance, the noise on the horizontal (or vertical) direction at high frequencies is higher than the noise at a radial direction of 45°. The DQE outcomes are slightly affected by the activation of the CRF filter. In fact, the CRF filter influences both the MTF and the NPS of the system, but in some way it seems not to affect too much its DQE. The effect of the filter is not substantial on the visibility of CDRAD details. As a matter of fact, no statistically significant differences were observed on the CD curves calculated by human observers when we activated the CRF filter.

V. CONCLUSION

In this paper, we have presented a physical and psychophysical characterization of a new clinical system (named AcSelerate) for digital radiography based on a thick a-Se layer (1000 μm). Despite the great thickness of its a-Se layer, the system presents an excellent MTF, which is to be expected with a detector based on direct conversion. On the other hand, the thick a-Se layer maintains a reasonably good QE at the harder beams encountered in general radiography, yielding good noise characteristics and a high DQE. As expected the RQA9 conditions give the lowest DQE.

We also compared results obtained with and without the use of a filter (named CRF) available with the AcSelerate system. The CRF filter influences both the MTF and NPS by decreasing the spatial resolution and the overall noise of the system, but it does lead to very small changes on DQE. Also the visibility of CDRAD details is basically unaltered, when the CRF filter is activated.

ACKNOWLEDGMENT

The authors are deeply indebted to Dr. G. Borasi for his guidance during all these years and for his precious encouragement and advice. The authors would also like to thank Satoshi Arakawa for his interest in the present work and Gregorio Benincasa for the assistance in the editing of the manuscript.

[a]Electronic mail: nico.lanconelli@unibo.it. Telephone:+39-051-2095136; Fax:+39-051-2095047.

[1]H. P. McAdams, E. Samei, J. Dobbins III, G. D. Tourassi, and C. E. Ravin, "Recent advances in chest radiography," Radiology **241**, 663–83 (2006).

[2]C. Schaefer-Prokop, U. Neitzel, H. W. Venema, M. Uffmann, and M. Prokop, "Digital chest radiography: An update on modern technology, dose containment and control of image quality," Eur. Radiol. **18**, 1818–1830 (2008).

[3]E. Samei and M. J. Flynn, "An experimental comparison of detector performance for direct and indirect digital radiography systems," Med. Phys. **30**(4), 608–622 (2003).

[4]K. Bacher, P. Smeets, L. Vereecken, An De Hauwere, P. Duyck, R. De Man, K. Verstraete, H. Thierens, "Image quality and radiation dose on digital chest imaging: comparison of amorphous silicon and amorphous selenium flat-panel systems," AJR Am. J. Roentgenol. **187**(3), 630–637 (2006).

[5]F. Nariyuki, S. Imai, H. Watano, T. Nabeta, and Y. Hosoi, "New development of large-area direct conversion detector for digital radiography using amorphous selenium with a C60-doped polymer layer," Proc. SPIE **7622**, 762240 (2010).

[6]International Electrotechnical Commission, "Medical electrical equipment—Characteristics of digital X-ray imaging devices—Part 1: Determination of the detective quantum efficiency," IEC-62220-1, Geneva, Switzerland, 2003.

[7]International Electrotechnical Commission, "Medical diagnostic x-ray equipment—Radiation conditions for use in the determination of characteristics," IEC-61267, Geneva, Switzerland, 2003.

[8]S. Rivetti, N. Lanconelli, R. Campanini, M. Bertolini, G. Borasi, A. Nitrosi, C. Danielli, L. Angelini, and S. Maggi, "Comparison of different commercial FFDM units by means of physical characterization and contrast-detail analysis," Med. Phys. **33**, 4198–4209 (2006).

[9]G. Borasi, E. Samei, M. Bertolini, A. Nitrosi, and D. Tassoni, "Contrast-detail analysis of three flat panel detectors for digital radiography," Med. Phys. **33**, 1707–1719 (2006).

[10]R. Aufricht, "Comparison of low contrast detectability between a digital amorphous silicon and a screen-film based imaging system for thoracic radiography," Med. Phys. **26**, 1349–1358 (1999).

[11]A. E. Burgess, "The Rose model, revisited," J. Opt. Soc. Am. A. **16**, 633–646 (1999).

[12]N. W. Marshall, "A comparison between objective and subjective image quality measurements for a full-field digital mammography system," Phys. Med. Biol. **51**, 2441–2463 (2006).

[13]S. Rivetti, N. Lanconelli, M. Bertolini, G. Borasi, P. Golinelli, D. Acchiappati, and E. Gallo, "Physical and psychophysical characterization of a novel clinical system for digital mammography," Med. Phys. **36**, 5139–5148 (2009).

[14]S. Rivetti, N. Lanconelli, M. Bertolini, A. Nitrosi, A. Burani, and D. Acchiappati, "Comparison of different computed radiography systems: Physical characterization and contrast detail analysis," Med. Phys. **37**, 440–448 (2010).

[15]G. Borasi, A. Nitrosi, P. Ferrari, and D. Tassoni, "On site evaluation of three flat panel detectors for digital radiography," Med. Phys. **30**, 1719–1731 (2003).

[16]P. Monnin, D. Gutierrez, S. Bulling, D. Lepori. J. F. Valley, and F. R. Verdun, "Performance comparison of an active matrix flat panel imager, computed radiography system, and a screen-film system at four standard radiation qualities," Med. Phys. **32**, 343–350 (2005).

[17]A. Mackenzie and I. D. Honey, "Characterization of noise sources for two generations of computed radiography systems using powder and crystalline photostimulable phosphors," Med. Phys. **34**, 3345–3357 (2007).

[18]L. Riccardi, M. C. Cauzzo, R. Fabbris, E. Tonini, and R. Righetto, "Comparison between a built-in "dual side," chest imaging device and a standard "single side," CR," Med. Phys. **34**, 119–126 (2007).